

# Precise measurement of $\alpha_K$ for the $M4$ transition from $^{193}\text{Ir}^m$ : A test of internal-conversion theory

N. Nica,\* J. C. Hardy, and V. E. Iacob  
*Cyclotron Institute, Texas A&M University, College Station, Texas 77843, USA*

S. Raman<sup>†</sup> and C. W. Nestor, Jr.  
*Oak Ridge National Laboratory, Oak Ridge, Tennessee 37830, USA*

M. B. Trzhaskovskaya  
*Petersburg Nuclear Physics Institute, Gatchina 188300, Russia*  
(Received 12 July 2004; published 4 November 2004)

The 10.5-day isomer in  $^{193}\text{Ir}$  decays by a single 80.2-keV  $M4$  transition directly to the ground state of that nucleus. We have measured the total intensity of  $K$  x rays relative to 80.2-keV  $\gamma$  rays for this transition to be 98.7(6). With the  $K$ -shell fluorescent yield for iridium taken to be 0.958(4), this result yields  $\alpha_K=103.0(8)$  for the  $K$ -shell internal conversion coefficient (ICC). The calculated  $\alpha_K$  for this transition is particularly sensitive to the treatment of the hole that is created by conversion in the atomic  $K$  shell. Recent ICC tables, which ignore the hole, yield  $\alpha_K=92.0$ . We demonstrate that calculations incorporating the hole produce values between 99.6 and 103.3 depending on the approximation used. Our result strongly supports the need to include the hole.

DOI: 10.1103/PhysRevC.70.054305

PACS number(s): 23.20.Nx, 27.80.+w

## I. INTRODUCTION

Internal conversion coefficients (ICCs) play an essential role in the analysis of nuclear decay schemes. They are used both in assigning spins and parities and in determining transition rates and branching ratios. For nearly 50 years, as theory and computational techniques evolved, successive tables of calculated ICC's have been readily available to users—see, for example, [1–4]. Comparisons of one table with another demonstrated consistency within a few percent for most transitions, and agreement with experiment appeared to be within a similar range. In most applications, higher precision than that was not demanded, and users have often taken required values from their table of choice without pausing to question too deeply the inherent uncertainties involved.

However, in 1973 a precision measurement ( $\pm 0.5\%$ ) on an  $M4$  transition in  $^{117}\text{Sn}$  and an accompanying survey of 15 other experimental ICCs for well-characterized  $E3$  and  $M4$  transitions [5] did point to a systematic discrepancy. When the experimental results were compared with the preferred calculation of the day [1], it was found that the theoretical values were systematically higher than experiment by 2%–3%. In the intervening 30 years, several new tables of ICCs have appeared and a modest number of ICCs have been determined experimentally, although unfortunately only a very few of the latter have claimed a precision even approaching 1%. When a new survey of world data by Raman *et al.* [6] appeared in 2002, the results reenforced the systematic discrepancy—now set firmly at 3%—previously noted between experiment and the tables of Hager and Seltzer [1],

and demonstrated that an almost identical discrepancy also existed between experiment and the more recent tables of Rösel *et al.* [2] and Band and Trzhaskovskaya [3]. Much better agreement was observed with the newest tables of Band *et al.* [4] where the exchange between electrons was treated exactly.

All ICC calculations to date have employed one of two extreme assumptions about the atomic subshell vacancy that occurs as a result of the conversion process. They assume either that the hole is filled instantaneously [2,4] or that the hole remains unfilled throughout the time that the conversion electron is present [1,3] in the atom. The problem of how to deal with the hole has been repeatedly discussed in the literature [6–11], where it was noted that both models have advantages and disadvantages. Nevertheless, simple physical arguments lead to the conclusion [10] that, for the bulk of transitions, the electron escapes from the atom in less time than it takes for the atomic hole to be filled. Surely, therefore, the hole should play a role in any ICC calculation.

In light of this expectation, a particularly intriguing outcome of the recent survey of ICC data was the apparent experimental preference for the “no hole” approximation made in the newest ICC calculations of Band *et al.* [4]. In producing their tables, the authors actually chose to disregard the hole entirely, based on an earlier comparison with experimental data [11], which indicated that better agreement with experimental ICCs would result. The survey of Raman *et al.* [6] confirmed this conclusion. They compared experimental data to the tabulated ICC values of Band *et al.* and also to values similarly computed, but with the hole included, and found that the former agreed to within a few tenths of a percent, while the latter disagreed by about 1%, theory again exceeding experiment as it had done for other tables in the past. On the one hand, it is impressive that such excellent agreement with experiment can be achieved; on the other, it

\*Electronic address: nica@comp.tamu.edu

<sup>†</sup>Deceased.

is troublesome that the agreement is only obtained at the price of ignoring the atomic hole.

Unfortunately, the body of world ICC data includes very few measurements of high precision—say,  $\leq 1\%$ . Consequently, it is only in the average over many different transitions that a discrepancy between experiment and theory at this level can be discerned at all, and it could be argued that the 1% difference in experimental agreement between the two calculations—one with the hole and the other without—is hardly a definitive test of one calculation's validity. Perhaps, too, there are other, previously masked deficiencies in the calculation that are playing a role at the 1% level. In any case, as higher precision is sought in  $\gamma$ -ray intensity calibration standards [12] and in  $\beta$ -decay branching ratios [13], it becomes increasingly important that we have a source of ICCs that can be depended on to 1% or better.

For an experiment to establish definitively which treatment of the atomic hole is best, what is required is an individual transition whose calculated ICC is particularly sensitive to the presence of the hole and which can be measured with high precision. In their 2002 survey, Raman *et al.* identified such a transition: the 80.2-keV *M4* isomeric decay of the second excited state in  $^{193}\text{Ir}$ . The transition energy is very close to the *K*-shell binding energy in iridium, which is at 76.112 keV [14], and consequently the value of the calculated *K*-shell ICC,  $\alpha_K$ , differs by more than 10% depending on whether the hole is incorporated in the calculation or not. The 10.5-day half-life of the isomer, its single-branch decay directly to the ground state, and the close proximity in energy of the transition's  $\gamma$  ray and the *K* x rays following internal conversion all lend themselves to a precise measurement. We report such a measurement here, in which we determine  $\alpha_K$  to  $\pm 0.8\%$ .

The experimental measurement and its analysis will be described in Secs. II and III, with sufficient detail provided to justify the precision we quote. In Sec. IV we will describe the calculation of ICCs, including two different approximations used to incorporate the hole in the atomic shell after conversion. Finally, in Sec. V we will discuss the impact of our result on the calculation and future use of ICCs.

## II. EXPERIMENT

The *K*-shell internal conversion coefficient  $\alpha_K$  for a particular transition is defined to be the ratio of the probability for internal conversion onto a *K*-shell electron relative to the probability for emitting a  $\gamma$  ray: viz.,  $\alpha_K = \lambda_{e_K} / \lambda_\gamma$ . Each electron vacancy created in the *K* shell produces *K* x rays with a probability equal to the *K*-shell fluorescent yield  $\omega_K$ . Thus, if only a single transition is involved and a spectrum of x rays and  $\gamma$  rays is recorded for its decay, the ratio of the total number of *K* x rays observed,  $N_K$ , to the total number of  $\gamma$  rays,  $N_\gamma$ , relates to the *K*-shell ICC by the simple relationship

$$\alpha_K \omega_K = \frac{N_K \epsilon_\gamma}{N_\gamma \epsilon_K}, \quad (1)$$

where  $\epsilon_\gamma$  and  $\epsilon_K$  are the detector efficiencies for the  $\gamma$  rays and x rays, respectively. Since fluorescent yields have been

reviewed recently [15] and are known rather precisely—typically to better than 0.5%—this allows  $\alpha_K$  to be extracted directly from measured peak areas provided that the detector efficiencies have been well calibrated.

The isomeric decay of the second excited state in  $^{193}\text{Ir}$  is a particularly fortunate case. It decays exclusively by a direct transition to the ground state, which is stable. Thus, the spectrum from the decay of a pure source exhibits only a single  $\gamma$ -ray peak together with x rays that correspond to this transition alone. Furthermore, the  $\gamma$ -ray energy of 80.236(7) keV is very close to the energy of the *K* x rays from iridium, 62–76 keV, so both groups can be observed in the same detector with virtually the same efficiency. Even so, to ensure the best possible precision, we used a germanium detector with state-of-the-art efficiency calibration. Our ORTEC Gamma-X HPGe detector—a 280-cm<sup>3</sup> *n*-type coaxial crystal—has been meticulously calibrated [16–18] to a relative precision of 0.15% (and 0.20% absolute) between 50 and 1400 keV. Its efficiency varies by less than 1.5% between 62 and 82 keV, the energy region of interest here.

With these advantages in hand, the main challenges of the measurement were to produce as pure a source of 10.5-day  $^{193}\text{Ir}^m$  as possible and to record its decay carefully over a long period of time in order to identify all remaining impurities. In what follows, we identify virtually all observed x- and  $\gamma$ -ray peaks and account for any that could interfere with the iridium transitions. We also take account of various small effects, such as coincident summing of *K $\alpha$*  and *L* x rays, and the contribution of germanium x rays escaping from the detector.

### A. Source preparation

The source was prepared from approximately  $\sim 70$  mg of highly enriched  $^{192}\text{Os}$  (99.935%) metal powder irradiated for 1 h at an effective 2200 m/s neutron flux of  $\sim 2 \times 10^{15}$  neutron/cm<sup>2</sup> s in the Hydraulic Tube Facility at the Oak Ridge High Flux Isotope Reactor. The  $^{193}\text{Ir}^m$  was produced via the reaction  $^{192}\text{Os}(n, \gamma)^{193}\text{Os}(\beta^-)^{193}\text{Ir}^m$ , in which  $^{193}\text{Os}$  has a  $\beta$ -decay half-life of 1.271 d. The irradiated osmium was allowed to decay for at least 10 days before the Os-Ir separation chemistry was begun. The irradiated osmium powder was then heated above 375 °C and air passed over it for 2 h. The bulk osmium was oxidized as volatile OsO<sub>4</sub>, carried out by the air flow and trapped, while the  $^{193}\text{Ir}^m$  was not volatilized and remained in the furnace vessel. The  $^{193}\text{Ir}^m$  was then dissolved in HNO<sub>3</sub> and its  $\gamma$ -ray spectrum recorded. This revealed that some osmium remained, with an Ir-to-Os activity ratio of  $\sim 200$ , and a second separation was required.

Hydrogen peroxide was then added to the Ir-Os nitrate solution in order to oxidize the residual osmium. The solution was slowly heated and purged with air to remove the volatile osmium oxide. The solution was gently dried down under a continuous air purge. Nitric acid was added to the dried-down solution and a sample taken for radio-assay. This time,  $\gamma$ -ray spectroscopic analysis showed no evidence of  $^{193}\text{Os}$  contamination in the  $^{193}\text{Ir}^m$  product.

Finally, the  $^{193}\text{Ir}^m$  solution was again evaporated to dryness and brought up again in HNO<sub>3</sub>. Small aliquots of the

volume-reduced  $^{193}\text{Ir}^m$  were repeatedly evaporated onto a 0.18-mm-thick tantalum disk and then covered with a thin aluminized Mylar film. The covered disk was mounted on an aluminum support 1.6 mm thick and secured with a 0.8-mm-thick aluminum frame. After the source had decayed, we used x-ray fluorescence to analyze this assembly and confirmed that its only important components were tantalum and aluminum.

Analysis of the decay spectra—to be described in the following sections—confirmed that the prepared source was free of  $^{191}\text{Os}$ , which could, in principle, have been produced by neutron capture on stable  $^{190}\text{Os}$  had there been any of that isotope in the irradiated material. Since the decay of  $^{191}\text{Os}$  also gives rise to iridium x rays, it was important to demonstrate that the purity of the original material and the selectivity of the chemical separation were sufficient to eliminate this possible contaminant.

### B. Radioactive decay analysis

Spectra were recorded at Texas A&M with our precisely calibrated HPGe detector and with the same electronics used in its calibration [17]. Our analog-to-digital converter was an Ortec TRUMP-8k/2k card controlled by the MAESTRO software. The TRUMP card uses the Gedcke-Hale method [19] to determine a live time that corrects for dead-time losses and random summing. The 8k-channel spectra covered the energy range from 10 keV to 2 MeV. In all, five source spectra and three background spectra were recorded over a total period of 98 days, nearly ten half-lives of  $^{193}\text{Ir}^m$ . The first three source spectra were successively recorded at intervals of roughly one iridium half-life, with each containing several million counts for the  $K$  x rays of iridium. Acquisition times ranged from 13 to 160 h. With one insignificant exception, our analysis did not find any isotope in the source with a half-life less than that of  $^{193}\text{Ir}^m$ . The last two source spectra were used to distinguish among the longer-lived impurities that were observed.

For the very first spectrum, the distance between the source and the front face of the detector was 151 mm, which is the distance at which the detector has been most precisely efficiency calibrated. All other spectra were recorded at 41 mm, in order to improve the acquisition rates as the source decayed. These distances were carefully set with a micrometer caliper, and were determined to  $\pm 0.2$  mm.

After subtraction of room background, the peak areas in each spectrum were determined with GF2, the least-squares peak-fitting program in the RADware series [20]. In doing so, we used the same fitting procedures as were used in the original efficiency calibration [17]. For the half-life analysis of impurity peaks, we divided the extracted areas by the live time and by the absolute detection efficiency to obtain absolute decay rates for each transition analyzed. In each case, a half-life was then obtained by a least-squares fit to the values obtained from the five recorded spectra.

### C. Efficiency calibration

The precise efficiency calibration of our HPGe detector at 151 mm [16–18] was based on measurements of 64  $\gamma$  rays

TABLE I. Monte Carlo calculated and measured efficiency ratios for the 151 mm source-detector distance relative to that for 41 mm. The first two columns list the isotopic sources used and their  $\gamma$ -ray energies, respectively. The last column gives the percentage difference between the calculated and measured efficiency ratios

Isotopic source	$\gamma$ -ray energy (keV)	Calculated efficiency ratio	Measured efficiency ratio	(Calculated-measured)/calculated
$^{241}\text{Am}$	59.5	0.1325(2)	0.1331(13)	-0.5(10)%
$^{57}\text{Co}$	122.1	0.1362(2)	0.1344(13)	1.3(10)%
$^{57}\text{Co}$	136.5	0.1368(2)	0.1353(15)	1.1(11)%

from 14 well-characterized sources and on Monte Carlo calculations with the CYLTRAN code [21], which incorporated the precisely determined properties of the detector [17]. Careful measurements were made and account taken of germanium x-ray escape at low energies [17] and positron annihilation in flight at high energies [18]. The Monte Carlo calculations showed *absolute* agreement with the measured efficiencies and thus demonstrated their effectiveness for interpolating efficiencies at energies between the measured calibration points. It was also demonstrated [17] that the same Monte Carlo calculations could describe the efficiency at a 1-m source-detector distance within  $\sim 1\%$ . For the present measurement, we needed to establish the validity of our efficiency calibration at 41 mm, the source-detector distance we used for most of our decay measurements. To do so in the energy interval of importance to the iridium measurements, we measured the 59.5-keV  $\gamma$  ray from  $^{241}\text{Am}$  and the 122.1- and 136.5-keV  $\gamma$  rays from  $^{57}\text{Co}$  at both 41 mm and 151 mm and obtained an experimental efficiency ratio; then we calculated the efficiency at both distances with the CYLTRAN code. The results appear in Table I.

It is important to note that, at 41 mm, the detector efficiency is considerably higher than at 151 mm, and the effects of coincidence summing become nearly an order of magnitude more important. In deriving the results quoted in column 4 of Table I, we applied corrections for  $\gamma$ - $\gamma$  and  $x$ - $\gamma$  summing, including x rays from both electron capture and conversion. This is a complicated procedure, which increases the quoted uncertainty considerably. A further increase arises because the 0.2-mm-distance measurement uncertainty is much more significant at 41 mm than it is at 151 mm. The last column of Table I shows the percentage differences between the calculated and experimental efficiency ratios. Within the quoted uncertainties, there is good agreement between measurements and Monte Carlo calculations. Consequently, we can confidently use Monte Carlo calculated efficiencies for 41 mm to investigate the decay and relative intensities of impurity activities in our source. Of course, the relative efficiencies at  $\sim 70$  keV and 80 keV, which are required in the application of Eq. (1), are known to 0.15% at our primary calibrated source-detector distance of 151 mm. The evident success of the Monte Carlo calculation at other distances indicates that we should also be able to apply it for those relative efficiencies at 41 mm with very little increase in uncertainty.

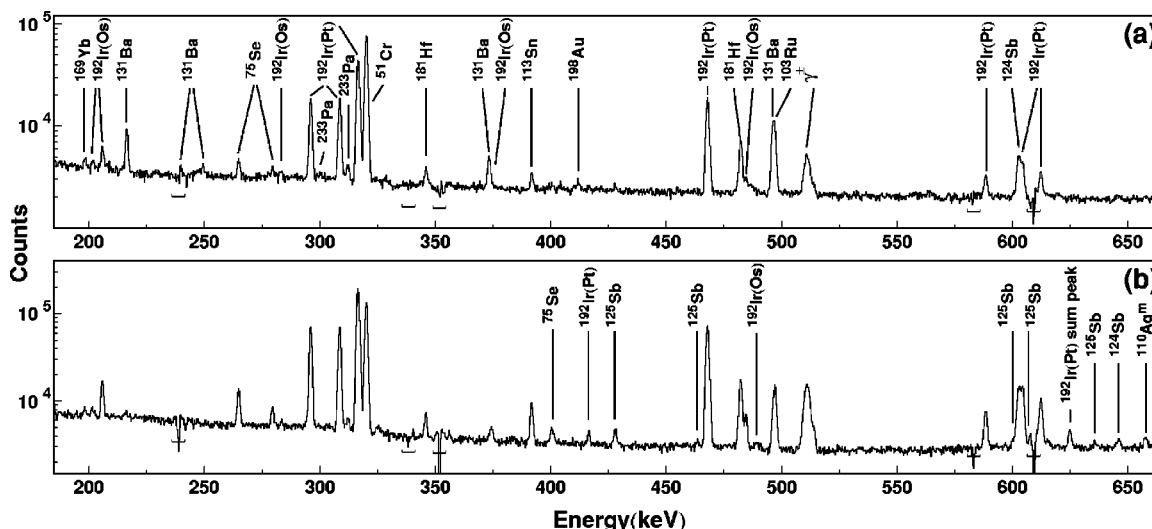


FIG. 1. A portion of the first [part (a)] and fourth [part (b)] background-subtracted  $\gamma$ -ray spectra, shown for the energy interval 200–700 keV. Peaks are identified by their  $\beta$ -decay parent and, where two daughter nuclei are possible, by the daughter in parentheses. The horizontal brackets located near the energy axis indicate regions where peaks in the subtracted background occur and anomalous fluctuations can thus be expected.

### III. ANALYSIS

The experimental analysis was done with two aims in mind. The first was to find any impurities that could interfere with the  $^{193}\text{Ir}^m$  x rays or the 80.2-keV  $\gamma$  ray. The second was to apply accurate procedures to such impurities in order to subtract their contribution to the peaks of interest.

#### A. Impurity identification

A complete survey was made of the five recorded source spectra. The energies and areas were obtained for all x- and  $\gamma$ -ray peaks with rates above a few hundredths of a percent of the  $^{193}\text{Ir}^m$  K x-ray rates. The decays of these peaks were followed in the five spectra and their sources identified by half-life and by observed relative  $\gamma$ -ray intensities. The results are illustrated in Fig. 1, where a region from 200 to 700 keV is shown from the first and fourth spectra. In this region, the most prominent groups of impurity  $\gamma$  rays, situated around 300 keV and just below 500 keV, come from

the decays of  $^{51}\text{Cr}$  and  $^{192}\text{Ir}$ . Other important  $\gamma$  rays seen in the spectra are those of  $^{181}\text{Hf}$ ,  $^{131}\text{Ba}$ , and  $^{124}\text{Sb}$ . Even the lowest-intensity transitions were analyzed and identified as, for example, those situated in the 200–300 keV interval, which are attributed to  $^{169}\text{Yb}$ ,  $^{75}\text{Se}$ , and  $^{233}\text{Pa}$ , as well as to other sources already identified from stronger peaks. An example of the decay curve obtained for an impurity  $\gamma$  ray—that of the 316.5-keV  $\gamma$  ray from the decay of  $^{192}\text{Ir}$ —is shown in Fig. 2(a).

Next, we determined the absolute activity for each identified parent based on the measured  $\gamma$ -decay rates and its known  $\gamma$ -emission probabilities [22]. A complete inventory of all identified impurities is presented in the first column of Table II. The next columns show the half-lives, the absolute parent activities, and the activities (in parts per million) relative to  $^{193}\text{Ir}^m$ . For clarity, we have expressed each derived activity as its value at the time that the first spectrum was recorded. The strongest contributor is  $^{51}\text{Cr}$ , which alone contributes more than two-thirds of the total impurity activity, yet it still is at the level of only 0.4% of the  $^{193}\text{Ir}^m$  activity.

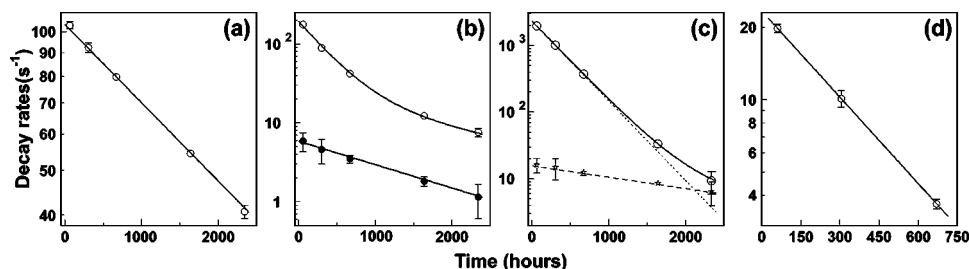


FIG. 2. Decay data (with uncertainties where large enough to be visible) for various peaks observed in our spectra. (a) The 316.5-keV peak from the  $^{192}\text{Ir}$  impurity decay. (b) The  $K_\alpha$  peak(s) from tantalum (open circles) and the tantalum  $K_\alpha$  component arising from the decay of  $^{181}\text{Hf}$  (solid circles) as derived from the observed  $^{181}\text{Hf}$   $\gamma$  rays. (c) The summed ( $K_\alpha + K_\beta$ ) peaks, mostly from the decay of  $^{193}\text{Ir}^m$  but still including the platinum and osmium x rays from the decay of the  $^{192}\text{Ir}$  impurity (circles); the summed ( $K_\alpha + K_\beta$ ) peaks from platinum and osmium alone as derived from the observed  $^{192}\text{Ir}$   $\gamma$  rays (diamonds). The lines are a two-component fit only to the upper points; note the excellent agreement with the lower points. (d) The 80.2-keV peak from the decay of  $^{193}\text{Ir}^m$ .

TABLE II. Identified impurities and their properties listed from higher- to lower-mass numbers. The absolute-activity values in column 3 and the relative activities in column 4 both are referred to the time at which the first spectrum was recorded. The observed activity for  $^{193}\text{Ir}^m$  is shown at the bottom for comparison.

Parent nucleus	$T_{1/2}$	Absolute activity (Bq)	Activity relative to $^{193}\text{Ir}^m$ (ppm)
$^{233}\text{Pa}$	27.0 d	5.9	14
$^{198}\text{Au}$	2.70 d	1.5	4
$^{192}\text{Ir}$	73.8 d	125	296
$^{181}\text{Hf}$	42.4 d	22.4	53
$^{169}\text{Yb}$	32.0 d	2.4	6
$^{155}\text{Eu}$	4.76 yr	5.1	12
$^{141}\text{Ce}$	32.5 d	4.6	11
$^{131}\text{Ba}$	11.5 d	46.3	110
$^{125}\text{Sb}$	2.76 yr	1.9	5
$^{124}\text{Sb}$	60.2 d	12.9	31
$^{113}\text{Sn}$	115 d	4.5	11
$^{110}\text{Ag}^m$	250 d	0.6	1
$^{103}\text{Ru}$	39.3 d	18.1	43
$^{75}\text{Se}$	120 d	4.2	10
$^{65}\text{Zn}$	244 d	92.7	220
$^{60}\text{Co}$	6.27 yr	32.9	78
$^{59}\text{Fe}$	44.5 d	1.5	3
$^{58}\text{Co}$	70.9 d	53.9	128
$^{54}\text{Mn}$	312 d	12.6	30
$^{51}\text{Cr}$	27.7 d	1850	4390
$^{46}\text{Sc}$	83.8 d	132	312
Summed impurities		2430	5,760
$^{193}\text{Ir}^m$	10.53 d	421000	

The next most prominent impurities are  $^{46}\text{Sc}$ ,  $^{192}\text{Ir}$ , and  $^{65}\text{Zn}$ , which are at 0.02% and below. Traces of the order of 1 ppm were detected for a few species, including the shortest-lived isotope  $^{198}\text{Au}$  ( $t_{1/2}=2.7$  d), which is the only observed impurity with a half-life shorter than that of  $^{193}\text{Ir}^m$ .

Very few  $\gamma$ -ray peaks recorded in our experimental spectra remained unidentified. The two most intense are at 158.9 keV and 1596.0 keV, having decay rates—activities cannot of course be determined for unidentified  $\gamma$  rays—relative to the  $^{193}\text{Ir}^m$ , ( $K_\alpha+K_\beta$ ) x rays of about 0.5% and 0.1%, respectively. The 158.9-keV peak could possibly be explained as the superposition of two close-lying  $\gamma$  rays coming from 13.6-day  $^{117}\text{Sn}^m$  and 119.7-day  $^{123}\text{Te}^m$ , both of which being producible from the neutron activation of a stable isotope. Neither isotope has  $\gamma$  or x rays that could contribute to our region of interest near the  $\gamma$  or x rays from  $^{193}\text{Ir}^m$ . We can advance no explanation for the 1596.0-keV  $\gamma$  ray but it is too weak to have any significant effect on our measurement.

Clearly, with all impurities contributing a total of  $\sim 0.6\%$  to the  $^{193}\text{Ir}^m$  activity in the first recorded spectrum, the purity

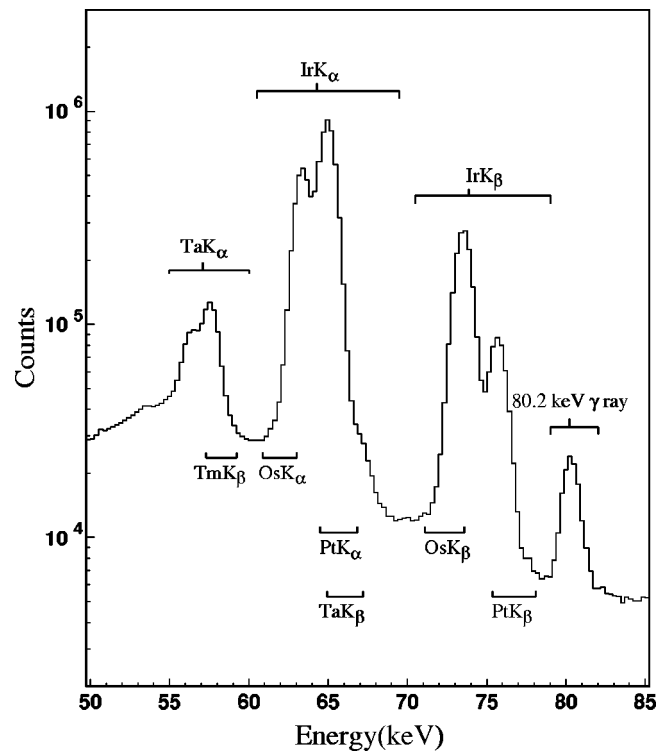


FIG. 3. A portion of the first recorded  $\gamma$ -ray spectrum, shown for the energy interval 50–85 keV. The strong clearly visible peaks are identified above the spectrum; the positions of small impurity contributions are indicated below the spectrum.

of the source is compatible with a precision measurement.

## B. Contributing impurities

Most of the impurities detected in our spectra do not interfere in any way with the iridium  $K_\alpha$  and  $K_\beta$  x rays or with the 80.2-keV  $\gamma$  ray from  $^{193}\text{Ir}^m$ . The region of interest for our  $^{193}\text{Ir}^m$  measurement is illustrated in Fig. 3 for the first spectrum. We considered the energy windows for potential interference to be 60.5–69.5 keV for the  $K_\alpha$  x rays, 70.5–79.0 keV for the  $K_\beta$  x rays, and 79.0–82.0 keV for the 80.2-keV  $\gamma$  ray and selected only those identified impurities that had x or  $\gamma$  rays within these energy windows. From their absolute decay rates we then calculated what contribution they make within these windows. The results are presented in Table III for the first, second, and third spectra, where we have separately tabulated the contributions to the two x-ray windows (upper part) and to the  $\gamma$ -ray window (lower part).

The impurities are ordered in the table by the size of their contributions. The most important one (2%–3%) affecting the  $K$  x rays comes from the Ta  $K_\beta$  x rays produced by fluorescence of the tantalum backing, principally caused by the  $K_\beta$  x rays from iridium that enter the target backing material. The next largest contribution comes from  $^{192}\text{Ir}$ , which exhibits both  $\beta^-$  and  $\text{EC}+\beta^+$  decay: the former generates Pt x rays, while the latter produces Os x rays. A much smaller contribution of Ta  $K_\beta$  x rays originates from  $^{181}\text{Hf}$   $\beta^-$  decay. These sources of Ta, Pt, and Os x rays are the only contributors of any real significance that we must take account of in

TABLE III. Impurities that can contribute to the peaks from  $^{193}\text{Ir}^m$ : the upper part lists those that can affect the summed ( $K_\alpha + K_\beta$ ) x rays, the bottom part those that can affect the 80.2-keV  $\gamma$  ray. The last three columns give the sizes of the contributions in the first, second, and third spectra, expressed as a percentage of the respective uncorrected peak areas.

Impurity	Type of contribution	Spectrum		
		First	Second	Third
Contribution to ( $K_\alpha + K_\beta$ ) x rays				
Ta <sup>a</sup>	Ta $K_\beta$	2.31%	2.16%	2.70%
$^{192}\text{Ir}$	Pt $K_\alpha + K_\beta$	0.57%	0.98%	2.28%
$^{192}\text{Ir}$	Os $K_\alpha + K_\beta$	0.24%	0.45%	0.96%
$^{181}\text{Hf}$	Ta $K_\beta$	0.08%	0.12%	0.24%
$^{169}\text{Yb}$	63.1-keV $\gamma$ ray	0.05%	0.08%	0.16%
$^{131}\text{Ba}$	78.3-keV $\gamma$ ray	0.02%	0.02%	0.02%
$^{233}\text{Pa}$	75.4-keV $\gamma$ ray	0.00%	0.01%	0.01%
$^{75}\text{Se}$	66.1-keV $\gamma$ ray	0.00%	0.00%	0.01%
Total impurities		3.28%	3.82%	6.38%
Contribution to 80.2-keV $\gamma$ ray				
$^{198}\text{Au}$	Hg $K_\beta$	0.037%	0.005%	0.000%
$^{75}\text{Se}$	80.9-keV $\gamma$ ray	0.002%	0.003%	0.008%
Total impurities		0.039%	0.008%	0.008%

<sup>a</sup>X-ray fluorescence of the tantalum backing.

analyzing the intensity of the ( $K_\alpha + K_\beta$ ) x rays from  $^{193}\text{Ir}^m$ . All other isotopes listed in the top part of Table III make tiny contributions, which in total amount to less than 0.2% of the  $^{193}\text{Ir}^m$  ( $K_\alpha + K_\beta$ ) x rays. The lower part of Table III shows an even more favorable situation for the window around the 80.2-keV  $\gamma$  ray. No major impurities were found to contribute here at all.

A different approach was also followed to cross-check the results of this impurity analysis. We considered all known radionuclides with half-lives from 1 d to 10 yr, searched for any among them that produce x- or  $\gamma$  rays in the  $^{193}\text{Ir}^m$  region of interest and then checked those cases to see if any of their other characteristic  $\gamma$  rays could be identified in our recorded spectra. This check is especially important for the 80.2-keV  $\gamma$ -ray peak, which, being relatively weak, could be seriously affected by an unrecognized impurity. Even though  $K_\beta$  x rays from Au and Hg as well as  $K_\alpha$  x rays from Po, At, and Rn could in principle contribute to the 80.2-keV  $\gamma$ -ray peak, no evidence was found of any possible candidate activities from among these elements. Indeed, except for trace amounts of  $^{233}\text{Pa}$  and  $^{198}\text{Au}$  noted in Table II, no other elements heavier than iridium were seen in our spectra. As to activities that might contribute  $\gamma$  rays to the region of interest, we found no evidence for them either, other than for  $^{75}\text{Se}$ , the effects of which we have already considered—see Table III.

We conclude that the list of contributing impurities in Table III can be considered complete. No other detectable impurities were found and, even if one exists, it could not conceivably contribute more than 0.1% to the coefficient  $\alpha_K$  being reported in this paper.

TABLE IV. Impurity corrections to the  $^{193}\text{Ir}^m$ 's ( $K_\alpha + K_\beta$ ) x rays (upper section) and 80.2-keV  $\gamma$  ray (middle section) for the first three spectra. The uncorrected decay rates are given in the first row of each section, followed by the percentage adjustments for each listed effect. The corrected decay rates appear in the last row of each section. The lower section presents the activity ratios and their average, together with the fluorescence yield  $\omega_K$  and our final value for  $\alpha_K$ .

	Spectrum		
	First	Second	Third
Ir ( $K_\alpha + K_\beta$ ) x rays			
Raw decay rate ( $\text{s}^{-1}$ )	1992.9(35)	1040.3(28)	387.1(5)
Ta $K_\beta$ x rays	2.41(2)%	2.48(3)%	3.19(2)%
Pt+Os ( $K_\alpha + K_\beta$ ) x rays	0.76(2)%	1.33(3)%	3.10(7)%
Minor impurities	0.08(1)%	0.11(1)%	0.20(1)%
Corrected decay rate ( $\text{s}^{-1}$ )	1928.2(35)	999.5(29)	362.1(6)
$^{193}\text{Ir}^m$ 80.2-keV $\gamma$ ray			
Raw decay rate ( $\text{s}^{-1}$ )	19.81(16)	10.13(16)	3.70(3)
Minor impurities	0.039(4)%	0.008(1)%	0.008(1)%
Corrected decay rate ( $\text{s}^{-1}$ )	19.80(16)	10.13(16)	3.70(3)
Ratios of ( $K_\alpha + K_\beta$ ) x rays to 80.2-keV $\gamma$ -rays			
	97.38(79)	98.6(16)	97.83(90)
Lorentzian correction		1.0(2)%	
Average ratio		98.7(6)	
Fluorescence yield $\omega_K^a$		0.958(4)	
Internal conversion coefficient $\alpha_K$ for 80.2-keV transition		103.0(8)	

<sup>a</sup>Reference [15].

### C. From peak ratio to $\alpha_K$

Having identified the impurities that contribute to the  $^{193}\text{Ir}^m$  peaks of interest in our spectra, we now turn to a quantitative evaluation of those contributions. With that in hand, we will then be able to determine the true activity values associated with  $^{193}\text{Ir}^m$  and extract the ratio of  $K$  x rays to 80.2-keV  $\gamma$  rays, from which the experimental value for  $\alpha_K$  can be derived. The corrections to the  $^{193}\text{Ir}^m$  x-ray and 80.2 keV  $\gamma$ -ray peaks are summarized for the first three spectra in Table IV, where the first row in each section of the table gives the uncorrected decay rate for the peak of interest, while the rows below list the percentage adjustment for each listed effect, culminating in the final corrected decay rate. We will deal with these effects in order. Note that in all cases we took careful account of Ge x-ray escape, both in correctly interpreting the detector's photopeak efficiency and in removing the contribution from the escape peaks themselves. The Ge x-ray escape ratios have been carefully measured for our detector [17] and decrease from 0.7% at 60 keV to 0.2% at 80 keV.

#### 1. Tantalum x rays

It can be seen from Fig. 3 that Ta  $K_\alpha$  x rays appear prominently between 55 and 60 keV. This, in itself, would not be a

problem, but it signals that the corresponding  $K_\beta$  x rays from Ta must lie under the important Ir  $K_\alpha$  peak. As already mentioned, these Ta x rays are mainly due to fluorescence in the Ta backing—an unfortunate choice as it turns out—but they also include a smaller contribution from the decay of the  $^{181}\text{Hf}$  impurity. Since the  $K$ -shell electron binding energy of Ta is 67.4 keV, all radiation that enters the backing and has energy greater than this value can lead to Ta  $K$  x rays through fluorescence. In our experiment, with a centroid energy of 73.9 keV, the Ir  $K_\beta$  x rays were the most intense cause for fluorescence, but other weaker  $\gamma$  rays at higher energy contributed too. This is demonstrated in Fig. 2(b), where the upper points (open circles) correspond to the total Ta  $K_\alpha$  decay rates and the lower ones (solid circles) to the contribution from  $^{181}\text{Hf}$  as calculated from the  $^{181}\text{Hf}$   $\gamma$  rays observed in our spectra. Evidently, in addition to the short-lived component in the upper decay (caused by  $^{193}\text{Ir}^m$  decay), there are longer-lived components in addition to the contribution from  $^{181}\text{Hf}$ .

Fortunately, we do not need to account for most of these contributions in detail because the intensity ratio of  $K_\beta$  to  $K_\alpha$  x rays is well established [23]. Based on the measured intensity of Ta  $K_\alpha$  x rays, we can use that ratio to establish the intensity of the Ta  $K_\beta$  x rays and then subtract the latter from the  $K_\alpha$  x rays of  $^{193}\text{Ir}^m$ . Before doing so, however, we first removed the contribution to the Ta  $K_\alpha$  peak from Tm x rays produced in the electron-capture decay of  $^{169}\text{Yb}$  (see Table II and Fig. 3): this represented 0.6%, 0.9%, and 1.4% of the total Ta  $K_\alpha$  peak area in the first three spectra, respectively. Then, we also incorporated the effects of coincident summing of the Ta  $K_\alpha$  and  $L$  x rays: this represented a loss of 0.26% and 2.1% from the Ta  $K_\alpha$  peak areas—and a corresponding gain to the Ta  $K_\beta$  peak areas—for the 151-mm and 41-mm source-detector distances, respectively. The total correction to the summed  $^{193}\text{Ir}^m$  ( $K_\alpha + K_\beta$ ) peak areas resulting from tantalum x rays ranges between 2.4% and 3.2%, as shown in Table IV.

### 2. Platinum and osmium x rays and other minor impurities

After Ta x rays, the second most important contributing impurity listed in Table III is  $^{192}\text{Ir}$ , because of which x rays of Pt and Os must underlie the  $^{193}\text{Ir}^m$  x rays. We used two independent methods to determine the contribution of  $^{192}\text{Ir}$  to the summed ( $K_\alpha + K_\beta$ ) peaks. The first was a half-life analysis. The upper points (circles) in Fig. 2(c) give the decay of the summed peaks *after* removal of the Ta  $K_\beta$  contribution. The lines represent the results of a least-squares fit to the points with two components fixed to the half-lives of  $^{192}\text{Ir}$  (73.8 d) and  $^{193}\text{Ir}^m$  (10.5 d). The second method was to calculate the total intensity of the Pt±Os x rays in each spectrum from the absolute activity of  $^{192}\text{Ir}$  (see Table II) as determined from the associated  $\gamma$  rays observed in the spectra. The black stars show the absolute decay rates determined in this manner. The points agree completely with the line determined from the lifetime fit to the summed peaks, confirming the consistency of the two methods and demonstrating that we have fully accounted for all significant impurities. The resulting corrections for the  $^{192}\text{Ir}$  impurity are listed in Table IV: they range from 0.8% to 3.1%.

The influence of the remaining impurities on the x-ray peaks and the 80.2-keV  $\gamma$  ray peak is more than an order of magnitude less than those we have discussed so far. In fact, for the most part they could be neglected. However, for completeness, we have calculated the contribution of the remaining impurities listed in Table III based on their absolute activities given in Table II. As seen in Table IV, their total effect on the x-ray peaks ranges from 0.1% to 0.2% and on the 80.2-keV  $\gamma$ -ray peak from 0.01% to 0.04%. Final confirmation that there are no significant impurities in the latter peak is given in Fig. 2(d) where no hint of a second component is evident in its decay.

### 3. Lorentzian correction

As described in Sec. II B, all peaks in our spectra were fitted with the GF2 program, which employs a Gaussian function (with tails and skewness available for inclusion) to match the measured peaks. While this achieves the necessary consistency with our efficiency-calibration procedures, it does not do justice to x-ray peaks, whose shapes reflect the finite widths of the atomic levels responsible for them. An x-ray peak is not fully described by a Gaussian function, but rather by the Voigt function, a convolution of the Lorentzian line profile with the Gaussian response function of the detector [24]. For this reason, compared to  $\gamma$  rays in the same energy region of the spectrum, x-ray peaks are wider and have tails that extend much farther both to higher and lower energy. Particularly because of the tails, an x-ray peak fitted even with a modified Gaussian function (plus background) will tend to underestimate the area of the peak by subsuming some of its tail into the presumed background. We determined a correction for this effect by the following procedure.

First, we established the parameters of the actual x-ray peak shape. The total width of the Lorentzian profile required for the Voigt function is the sum of initial and final atomic level widths; we used the values for the elements of interest taken from Refs. [24,25]. The width of the Gaussian detector response function was obtained from the measured width of the 80.2-keV  $\gamma$  ray in our spectrum.

Next, using Voigt functions with these determined parameters, we generated a simulated x-ray spectrum in the energy interval 0–128.6 keV incorporating the  $K_\alpha$  and  $K_\beta$  x-ray components of Ir, Ta, Pt, and Os, with the same relative intensities and counting statistics as we obtained in the first spectrum of our data. We also included the smoothed “step functions” characteristic of a germanium detector’s response function with each peak. This spectrum then closely simulated the real spectrum but with one important difference: the peak areas were known exactly.

Finally, we analyzed this simulated spectrum with GF2 using exactly the same procedures as those we used for the real spectrum. The area we obtained for the summed Ir  $K_\alpha$  and  $K_\beta$  x-ray peaks was 1.0(2)% less than the sum of the known (input) areas of these peaks. We verified that for a simulated (Gaussian) 80-keV  $\gamma$ -ray peak, the area obtained from GF2 agreed well with the known area in that case. We consider that this 1.0% correction factor is common to all three spectra shown in Table IV and thus apply it to the peak

ratio obtained *after* the results from the three spectra have been averaged together.

#### 4. Conversion coefficient

Throughout this analysis, we have always considered the sum of the Ir  $K_\alpha$  and  $K_\beta$  peaks. It is, of course, the sum that is required in the eventual evaluation of  $\alpha_K$  but, in addition, by considering only the sum, we avoid having to account for coincidence summing between the  $K_\alpha$  and  $L$  x rays since what is lost to the  $K_\alpha$  peak is gained by the  $K_\beta$  peak and the sum remains the same. Thus, after the spectrum-dependent corrections itemized in Table IV have been applied, we extract the ratio of  $K$  x rays to the 80.2-keV  $\gamma$  ray from each of the three spectra. Since the impurities are so well under control and the corrections to account for them are so small, the overall uncertainties on the peak ratios are dominated by counting statistics and peak-fitting uncertainties. As seen in the table, the three spectra yield statistically consistent values for the peak ratio, so we have taken a weighted average and applied the Lorentzian correction to that average to get the final result for the peak ratio, 98.7(6), shown there. Taking this result together with the  $K$ -shell fluorescent yield tabulated in Ref. [15], we obtain a value for the 80.2-keV  $M4$  transition from  $^{193}\text{Ir}^m$  of  $\alpha_K=103.0(8)$ .

Our result for  $\alpha_K$  can now be compared with two previous measurements that claimed comparable precision: Lindner *et al.* [26] obtained 104(3), in complete agreement with our result, and Zheltonozhskii *et al.* [27] claimed 92.6(9), in serious disagreement. Impurities clearly played a greater role in both these measurements and, as far as one can tell from the publications, in neither case were these impurities investigated as exhaustively as in our work. Lindner *et al.* are more convincing, however, in dealing with what they do identify: they see quite strong Os and Pt x rays in their spectrum from the decay of  $^{192}\text{Ir}$ , which they can readily correct for. In contrast, Zheltonozhskii *et al.* admit the presence of  $^{191}\text{Os}$ , which would lead to Ir x rays indistinguishable from those arising from  $^{193}\text{Ir}^m$  decay, but they give no indication of how they correct for them. Efficiency calibration of their  $\gamma$ -ray detector was also handled more thoroughly by Lindner *et al.* who used 14 calibrated sources with a total of 30 x- and  $\gamma$ -ray lines; Zheltonozhskii *et al.* relied on a single source—presumably  $^{182}\text{Ta}$ , although it is identified as  $^{192}\text{Ta}$  in Ref. [27]—the intensities of whose  $\gamma$  rays are not particularly well known below 100 keV. We conclude that there are plausible reasons to believe that the measurement of Zheltonozhskii *et al.* is flawed. Since our present result agrees with that of Lindner *et al.* but is nearly a factor of 4 more precise, we will adopt our result, unaveraged with the others, and proceed to compare it with theory.

#### IV. THEORY

We have calculated theoretical values of the ICC in the first nonvanishing order of perturbation theory using the one-electron approximation [28–30]. Calculations were performed for a free neutral atom with a spherically symmetric potential. Relativistic electron wave functions required for the conversion matrix elements were obtained in the frame-

work of the Dirac-Fock method, where the exchange interactions between atomic electrons and between these electrons and the conversion electron receding to infinity during the conversion process were treated exactly [4]. In the wave function calculations, the static effect of the nuclear finite size was taken into account under the assumption that the static charge is distributed homogeneously over the volume of a sphere with radius  $R_0=1.2A^{1/3}$  fm, where  $A$  is the mass number. The dynamic effect of the nuclear finite size (the penetration effect) was considered in the surface-current (SC) model [31]. In the continuum wave function calculations, we used the experimental value for the binding energy of the  $K$  shell in the iridium atom, which is 76.112 keV [14].

The expression for internal conversion of an  $M4$  transition on the  $ns_{1/2}$  shell, where  $n$  is the principal quantum number, can readily be derived from the general ICC expressions [4,6,30] and takes the following form:

$$\alpha_{i=ns_{1/2}}^{M4} = \sum_{\kappa_f=-4,+5} |\mathcal{M}_{if}^{M4}|^2 = \frac{2}{9} \pi k \alpha (5|R_{if}|_{\kappa_f=-4}^2 + 4|R_{if}|_{\kappa_f=+5}^2), \quad (2)$$

where the radial integral  $R_{if}$  is written as

$$R_{if} = \int_0^\infty [G_i(r)F_f(r) + F_i(r)G_f(r)]X_4(kr)dr. \quad (3)$$

In Eq. (2),  $\kappa$  is the relativistic quantum number  $\kappa = (\ell - j)(2j + 1)$ , where  $\ell$  and  $j$  are the orbital and total angular momentum of an electron, respectively. Index  $i$  refers to the initial (bound) state of an electron, and index  $f$  applies to the final (free) electron state. Recall that for the  $K$  shell ( $1s_{1/2}$  shell)  $\kappa_i = -1$ . The matrix element of the  $M4$  conversion transition is denoted by  $\mathcal{M}_{if}^{M4}$ . The summation in Eq. (2) extends over all permissible final states. In the case in question, there are two values of  $\kappa_f = -4, +5$  allowed by the selection rules. The  $\gamma$ -ray energy is designated by  $k$ , and  $\alpha$  is the fine structure constant. All expressions in this work make use of relativistic units ( $\hbar = m_0 = c = 1$ ).

The major  $G(r)$  and minor  $F(r)$  components of the relativistic radial electron wave function are normalized to unity for the bound state,

$$\int_0^\infty [G_i^2(r) + F_i^2(r)]dr = 1, \quad (4)$$

and per unit energy range for the continuum state to give

$$\lim_{r \rightarrow \infty} \left[ G_f^2(r) + \frac{E+1}{E-1} F_f^2(r) \right] = \frac{1}{\pi} \sqrt{\frac{E+1}{E-1}}. \quad (5)$$

In Eq. (5),  $E$  is the total energy of the conversion electron including the rest mass. The radial part of the transition potential in the SC model can be written as

$$X_4(kr) = \begin{cases} j_4(kr) \frac{h_4(kR_0)}{j_4(kR_0)} & \text{for } r \leq R_0, \\ h_4(kr) & \text{for } r > R_0, \end{cases} \quad (6)$$

where  $j_4(kr)$  and  $h_4(kr)$  are the spherical Bessel and Hankel functions of the fourth order, respectively.

The 80.2-keV  $M4$  transition from  $^{193}\text{Ir}^m$  is an unhindered one. Since its Weisskopf hindrance factor  $F_W$  is  $\approx 2$  [6], the occurrence of anomalies in its ICC due to the penetration effect is practically ruled out [30]. Nevertheless, to make an estimate of the penetration effect, we calculated the ICC  $\alpha_K^{M4}$  for the transition from  $^{193}\text{Ir}^m$  using both the SC model, where the effect is taken into account approximately, and the so-called “no penetration” (NP) model, where the effect is ignored [28]. The difference between these two calculations is 1.8%. We believe that the SC model is more appropriate to the physical situation because the infinities at the origin for the nuclear transition potentials are eliminated in this model. As shown in [6,10], the SC model generally allows one to obtain ICC values which are closer to experimental data than ICC values obtained using the NP model.

The problem of whether or not to take into account the hole in the atomic shell after conversion has been considered in a number of papers both with respect to the validity of the ICC theory (see, for example, [10]) and to the quality of agreement between that theory and experimental data [6,11]. If the hole is disregarded, the electron wave functions of the initial and final states are calculated in the same self-consistent field (SCF) of the neutral atom. Otherwise, if the hole is included, the bound wave function is computed in the neutral atom SCF while the continuum wave function is calculated in the field of the ion, which has a vacancy in the atomic subshell from which the conversion electron was emitted. We included the hole in two alternative ways: (1) We used the frozen orbital approximation, in which the continuum wave function is calculated in the ion field constructed from the bound wave functions of the neutral atom; this assumes that the hole is unfilled and the atomic orbitals have no time to rearrange after the electron’s removal. (2) We used continuum wave functions calculated in the SCF of the ion, assuming full relaxation of the ion orbitals.

The problem of how to take the hole into account is connected with the relationship between the time scale for filling the hole and the residence time of the conversion electron in the atom. If the width of the  $K$  level in iridium is  $\Gamma \approx 40$  eV [25], it follows that the average time for filling the hole is  $\sim 2 \times 10^{-17}$  s. The time it takes for the electron to escape the iridium atom is  $\sim 2 \times 10^{-18}$  s. Thus, based on these albeit rough estimates, the hole should be included from physical considerations. However, in doing so, it should be kept in mind that the expressions for ICC have been obtained in the framework of perturbation theory under the assumption that the matrix element of the energy perturbation is calculated using unperturbed wave functions. So when we take the hole into consideration, difficulties emerge from the possible nonorthogonality of wave functions calculated in the different atomic fields.

In using the SCF calculation to incorporate the hole, we also tried a variant in which we treated the effect of relaxation of electron orbitals as a consequence of the nonorthogonality between wave functions of the initial and final states of the atom. The appropriate correction is known as the “exchange and overlap effect” (not to be confused with electron exchange in the SCF calculations), by analogy with the electron capture process. The exchange and overlap effect has been considered for the conversion process in [32]

TABLE V. Theoretical values of  $\alpha_K^{M4}$  for  $^{193}\text{Ir}^m$  calculated in various models; also listed are the corresponding deviations  $\Delta$  from the experimental result obtained in this work,  $\alpha_K^{M4} = 103.0(8)$ .

Model	$\alpha_K^{M4}$	$\Delta$ , %
No hole	92.0(3)	10.7(8)
Hole, frozen orbitals	103.3(3)	-0.3(8)
Hole, SCF of ion	99.6(3)	3.3(8)
Hole, SCF of ion corrected <sup>a</sup>	99.7(3)	3.2(8)

<sup>a</sup>Including “exchange and overlap.”

using the sudden approximation. According to expressions obtained in [32], the ICC  $\alpha_K^{M4}(\text{cor})$  corrected for the exchange and overlap may be written as follows:

$$\alpha_K^{M4}(\text{cor}) = \sum_{\kappa_f=-4,+5} \left| \mathcal{M}_{1s_{1/2}'}^{M4} - \sum_{n \neq 1} \mathcal{M}_{ns_{1/2}'}^{M4} \frac{\langle (ns_{1/2}')' | 1s_{1/2} \rangle}{\langle (ns_{1/2}')' | ns_{1/2} \rangle} \right|^2. \quad (7)$$

Here  $\mathcal{M}_{ns_{1/2}'}^{M4}$  are the matrix elements of the  $M4$  transition for conversion on all shells with the same  $\kappa_f$ —i.e., on all the  $ns_{1/2}$  shells ( $n=2,3,\dots,6$  for the iridium atom)—calculated at the same energy  $E_k$  of the conversion electron as was used in the case of the  $K$  shell. The overlap integrals  $\langle (ns_{1/2}')' | 1s_{1/2} \rangle$  and  $\langle (ns_{1/2}')' | ns_{1/2} \rangle$  are taken between primed wave functions, which are those calculated in the Dirac-Fock SCF of the ion with the  $K$ -shell hole, and the unprimed wave functions, which are those computed in the Dirac-Fock SCF of the neutral atom.

Calculated values of  $\alpha_K^{M4}$  are presented in the second column of Table V. The value in the first row effectively is the one that would be derived from the recently published tables of Band *et al.* [4]. The three other rows give values that were calculated with the hole included under the approximations just described. To obtain these results, we used the value 80.22(2) keV [26] for the  $^{193}\text{Ir}^m$  transition energy. The experimental uncertainty in this number is reflected in the uncertainties quoted on the theoretical values of  $\alpha_K^{M4}$  in the table.

It is evident from the table that the conversion coefficients obtained with the  $K$ -shell hole included in the calculation differ by about 10% from the value obtained when the hole is ignored. However, the two different approximations used to incorporate the effect of the hole lead to results that differ from one another by  $\sim 3.5\%$ . The exchange and overlap correction has a relatively small effect, increasing the ICC by only 0.15%.

## V. CONCLUSIONS

The third column in Table V shows the percentage difference between the various calculated conversion coefficients and the value,  $\alpha_K^{M4}(\text{expt}) = 103.0(8)$  obtained in this work. We denote the difference as follows:

$$\Delta = \frac{\alpha_K^{M4}(\text{expt}) - \alpha_K^{M4}(\text{theor})}{\alpha_K^{M4}(\text{expt})} \times 100\%. \quad (8)$$

From these percentage differences we can conclude that our experimental result rules out the calculation that ignores effects from the  $K$ -shell hole on the  $K$ -conversion coefficient. Furthermore, we demonstrate much better agreement with the result from the “frozen orbitals” approximation than with the results obtained from a calculation of the final-state wave functions in the self-consistent field of the ion.

Of course, we chose this particular  $^{193}\text{Ir}^m$  transition because its  $\alpha_K$  value is extremely sensitive to the presence or absence of a  $K$ -shell hole in the ICC calculation. The effect of including the hole increases with decreasing energy  $E_k$  of the conversion electron. Furthermore, energy for energy, the hole effect is the largest for  $K$ -shell conversion coefficients and for high multipolarity transitions. Our case of  $K$ -shell conversion, with a high transition multipolarity  $L=4$  and low energy  $E_k=4.11$  keV, really maximizes the hole effect. Thus, although we have clearly shown that for  $^{193}\text{Ir}^m$  a serious discrepancy results from ignoring the hole in a calculation of  $\alpha_K$ , much smaller discrepancies will characterize the major-

ity of transitions for which ICCs are required.

Although our result is quite definitive for the transition studied, naturally with a single measurement we cannot rule out the possibility that other unidentified theoretical factors are playing a role in this particular case. We plan to measure ICCs for other sensitive transitions with different multiplicities and in nuclei from different mass regions in order to ensure that our conclusions are universally applicable.

#### ACKNOWLEDGMENTS

We are very grateful to C.W. Alexander and his colleagues at Oak Ridge National Laboratory for their very thorough and successful chemical purification of our source after it emerged from the reactor. We should also like to thank Dr. Henry Griffin for asking the right questions about some of the details of our analysis. The work of the Texas A&M authors is supported by the U.S. Department of Energy under Grant No. DE-FG03-93ER40773 and by the Robert A. Welch Foundation. The work of M.T. is supported by the Russian Foundation for Basic Research under Grant No. 02-02-17117 and U.S. Defense Threat Reduction Agency Contract No. DTRA01 01-P-0134.

- 
- [1] R.S. Hager and E.C. Seltzer, Nucl. Data, Sect. A **4**, 1 (1968).  
 [2] F. Rösel, H.M. Fries, K. Alder, and H.C. Pauli, At. Data Nucl. Data Tables **21**, 91 (1978).  
 [3] I.M. Band and M.B. Trzhaskovskaya, *Tables of Gamma Ray Internal Conversion Coefficients for K, L and M Shells*, 10  $\leq Z \leq 104$ , Leningrad Nuclear Physics Institute report, 1978 (in Russian).  
 [4] I.M. Band, M.B. Trzhaskovskaya, C.W. Nestor, Jr., P. Tikkanen, and S. Raman, At. Data Nucl. Data Tables **81**, 1 (2002).  
 [5] S. Raman, T.A. Walkiewicz, R. Gunnink, and B. Martin, Phys. Rev. C **7**, 2531 (1973).  
 [6] S. Raman, C.W. Nestor, Jr., A. Ichihara, and M.B. Trzhaskovskaya, Phys. Rev. C **66**, 044312 (2002).  
 [7] I.M. Band, V.I. Fomichev, and M.B. Trzhaskovskaya, J. Phys. B **12**, 3187 (1979).  
 [8] I.M. Band, M.A. Listengarten, and M.B. Trzhaskovskaya, Bull. Acad. Sci. USSR, Phys. Ser. (Engl. Transl.) **45**, 139 (1981).  
 [9] I.M. Band and M.B. Trzhaskovskaya, Bull. Acad. Sci. USSR, Phys. Ser. (Engl. Transl.) **55**, 59 (1991).  
 [10] M.A. Listengarten and V.O. Sergeev, in *Proceedings of the IX Workshop on Nuclear Physics*, Bukhara, Uzbekistan, 1979, edited by V.P. Prikhodceva (Nauka, Leningrad, 1981), p. 39 (in Russian).  
 [11] I.M. Band and M.B. Trzhaskovskaya, At. Data Nucl. Data Tables **55**, 43 (1993).  
 [12] IAEA-TECDOC-619, x-ray and gamma-ray standards for detector calibration, International Atomic Energy Agency, 1991, and an updated version to be published soon.  
 [13] J.C. Hardy, V.E. Iacob, M. Sanchez-Vega, R.G. Neilson, A. Azhari, C.A. Gagliardi, V.E. Mayes, X. Tang, L. Trache, and R.E. Tribble, Phys. Rev. Lett. **91**, 082501 (2003).  
 [14] R.D. Deslattes *et al.*, Rev. Mod. Phys. **75**, 35 (2003).  
 [15] E. Schönfeld and H. Janssen, Nucl. Instrum. Methods Phys. Res. A **369**, 527 (1996).  
 [16] J.C. Hardy, V.E. Iacob, M. Sanchez-Vega, R.T. Effinger, P. Lipnik, V.E. Mayes, D.K. Willis, and R.G. Helmer, Appl. Radiat. Isot. **56**, 65 (2002).  
 [17] R.G. Helmer, J.C. Hardy, V.E. Iacob, M. Sanchez-Vega, R.G. Neilson, and J. Nelson, Nucl. Instrum. Methods Phys. Res. A **511**, 360 (2003).  
 [18] R.G. Helmer, N. Nica, J.C. Hardy, and V.E. Iacob, Appl. Radiat. Isot. **60**, 173 (2004).  
 [19] R. Jenkins, R.W. Gould, and D. Gedcke, *Quantitative X-ray Spectroscopy* (Marcel Dekker, New York, 1981), p. 266.  
 [20] D. Radford (private communication).  
 [21] J.A. Halbleib and T.A. Mehlhorn, Nucl. Sci. Eng. **92**, 338 (1986).  
 [22] Evaluated Nuclear Structure Data File maintained by the National Nuclear Data Center, Brookhaven National Laboratory: <http://www.nndc.bnl.gov>; The Isotopes Project, Lawrence Berkeley National Laboratory: <http://www.isotopes.lbl.gov>.  
 [23] E. Schönfeld and G. Rodloff, Physikalisch-Technische Bundesanstalt, Report No. PTB-6.11-1999-1, Braunschweig, 1999.  
 [24] Klaus Debertin and Richard Helmer, *Gamma- and X-ray Spectrometry with Semiconductor Detectors* (Elsevier, Amsterdam, 2001).  
 [25] O. Kerki-Rahkonen and M. Krause, At. Data Nucl. Data Tables **14**, 139 (1974).  
 [26] M. Lindner, R. Gunnink, and R.J. Nagle, Phys. Rev. C **36**, 1132 (1987).

- [27] V.A. Zheltonozhskii, P.N. Muzalev, A.F. Novgorodov, and M.A. Ukhin, *Sov. Phys. JETP* **67**, 16 (1988).
- [28] M.E. Rose, in *Internal Conversion Processes*, edited by J.H. Hamilton (Academic, New York, 1966), p. 15.
- [29] H.C. Pauli, K. Alder, and R. Steffen, *The Electromagnetic Interaction in Nuclear Spectroscopy* (North-Holland, Amsterdam, 1975), p. 341.
- [30] I.M. Band, M.A. Listengarten, and A.P. Feresin, *Anomalies in Internal Conversion Coefficients of Gamma-Rays* (Nauka, Leningrad, 1976) (in Russian).
- [31] L.A. Sliv, *Zh. Eksp. Teor. Fiz.* **21**, 770 (1951).
- [32] M.A. Listengarten, I.M. Band, and M.B. Trzhaskovskaya, *Izv. Akad. Nauk SSSR, Ser. Fiz.* **49**, 2195 (1985); [*Bull. Acad. Sci. USSR, Phys. Ser. (Engl. Transl.)* **49**, 105 (1985)].